

# A post-Newtonian diagnosis of quasiequilibrium configurations of neutron star-neutron star and neutron star-black hole binaries

Emanuele Berti,<sup>\*</sup> Sai Iyer,<sup>†</sup> and Clifford M. Will<sup>‡</sup>  
*McDonnell Center for the Space Sciences, Department of Physics,  
 Washington University, St. Louis, Missouri 63130, USA*

We use a post-Newtonian diagnostic tool to examine numerically generated quasiequilibrium initial data sets for non-spinning double neutron star and neutron star-black hole binary systems. The PN equations include the effects of tidal interactions, parametrized by the compactness of the neutron stars and by suitable values of “apsidal” constants, which measure the degree of distortion of stars subjected to tidal forces. We find that the post-Newtonian diagnostic agrees well with the double neutron star initial data, typically to better than half a percent except where tidal distortions are becoming extreme. We show that the differences could be interpreted as representing small residual eccentricity in the initial orbits. In comparing the diagnostic with preliminary numerical data on neutron star-black hole binaries, we find less agreement.

## I. INTRODUCTION AND SUMMARY

Advances in numerical general relativity have made it possible to solve Einstein’s equations for the astrophysically important problem of the inspiral and merger of binary systems of compact bodies (black holes or neutron stars) with unprecedented accuracy and robustness, both in the initial data obtained from Einstein’s equations, and in the subsequent time evolution of the system. Work is ongoing to stitch together results from post-Newtonian theory, which accurately describes the early part of the inspiral, with numerical relativity, which describes the final few orbits, merger and ringdown of the final black hole, in an effort to develop a complete description of the evolution and gravitational-wave emission from such systems that can be used effectively in analysis of data from gravitational-wave interferometers [1, 2, 3, 4].

As part of this program to link post-Newtonian theory with numerical relativity, we proposed and developed a diagnostic tool, based on the post-Newtonian (PN) approximation, for analysing numerical relativity initial data sets for compact binaries [5, 6, 7]. Recall that the post-Newtonian approximation is effectively an expansion of Einstein’s theory in powers of a small parameter  $\epsilon \sim (v/c)^2 \sim Gm/rc^2$ .

Numerical data sets, obtained from solutions of the initial-value equations of general relativity, are generally configured to represent the quasicircular orbit of a compact binary system late in its inspiral phase, when the bodies have only a few orbits remaining before merger. Such a quasicircular orbit (circular, apart from the radiation-induced inspiral) is the expected end-point of evolution of a compact binary system under the circularizing effect of gravitational radiation reaction in the absence of external perturbations.

The PN diagnostic provides analytic expressions for the total binding energy (the difference between the total gravitational mass of the system and that of the two stars in isolation) and angular momentum of the system as a function of its orbital angular velocity, and allows for arbitrary mass ratios, spins, finite-size effects such as tidal interactions, and a non-zero orbital eccentricity. We found that the PN expressions for circular orbits agreed with the numerical relativity results surprisingly well (see also [8]), even for orbital separations in a highly relativistic regime where  $\epsilon$  is not so small, but that there were systematic differences that could not be blithely attributed to errors in either the PN approximation or the numerical data.

For binary black hole initial data, for example, we found [5, 7] that our diagnostic gave a better fit to the numerical data from several groups if the orbital eccentricity were allowed to be non-zero, with values as large as 0.03. Here the bodies were viewed as residing initially at the apocenter of the orbit, in keeping with the constraint built into the numerical initial data that the bodies be moving perpendicularly to their separation. And indeed, subsequent calculations of the time evolution of these initial data using numerical relativity showed that the orbits *were* slightly eccentric, with values of eccentricity agreeing in order of magnitude with those predicted by the PN diagnostic (see, eg. [9]). Efforts are now being made to “tweak” the initial data for binary black holes in order to achieve orbits that more nearly approximate the expected quasicircular orbits [10, 11, 12].

---

<sup>\*</sup>berti@wugrav.wustl.edu

<sup>†</sup>sai@wugrav.wustl.edu

<sup>‡</sup>cmw@wuphys.wustl.edu

In this paper we turn our attention to binary systems containing non-rotating neutron stars (NS). In [6] we applied the diagnostic to one neutron star binary initial data set for corotating stars obtained by Miller *et al.* [13], but here we focus on an extensive set of *non-spinning* neutron star initial data obtained by Taniguchi *et al.* [14, 15, 16], including both equal-mass and unequal-mass systems; and on preliminary initial data sets for neutron star-black hole binaries obtained by Taniguchi *et al.* [17, 18, 19] and Grandclément [20].

While for black holes, tidal effects are negligible at the separations in question, for neutron stars, tidally induced distortions must be taken into account (see [6] for discussion). These effects depend on the size of the neutron star, as encoded in a “compactness” factor,  $M/R$ , where  $M$  and  $R$  represent mass and radius, and on a set of “apsidal constants”,  $k_l$ , which measure the degree of distortion of the body as a result of an external tidal force, for each multipole order  $l$ . These are also known as “Love numbers” in other contexts. The apsidal constants depend on the equation of state (EOS) used to model the neutron star interiors.

For given values of the masses, compactness parameters, apsidal constants and eccentricity, the PN expressions for binding energy and angular momentum can be evaluated and compared with the data. Alternatively, for example, one can leave the eccentricity as a free parameter and solve for that value that gives the best agreement between the PN and the numerical results for the given angular velocity.

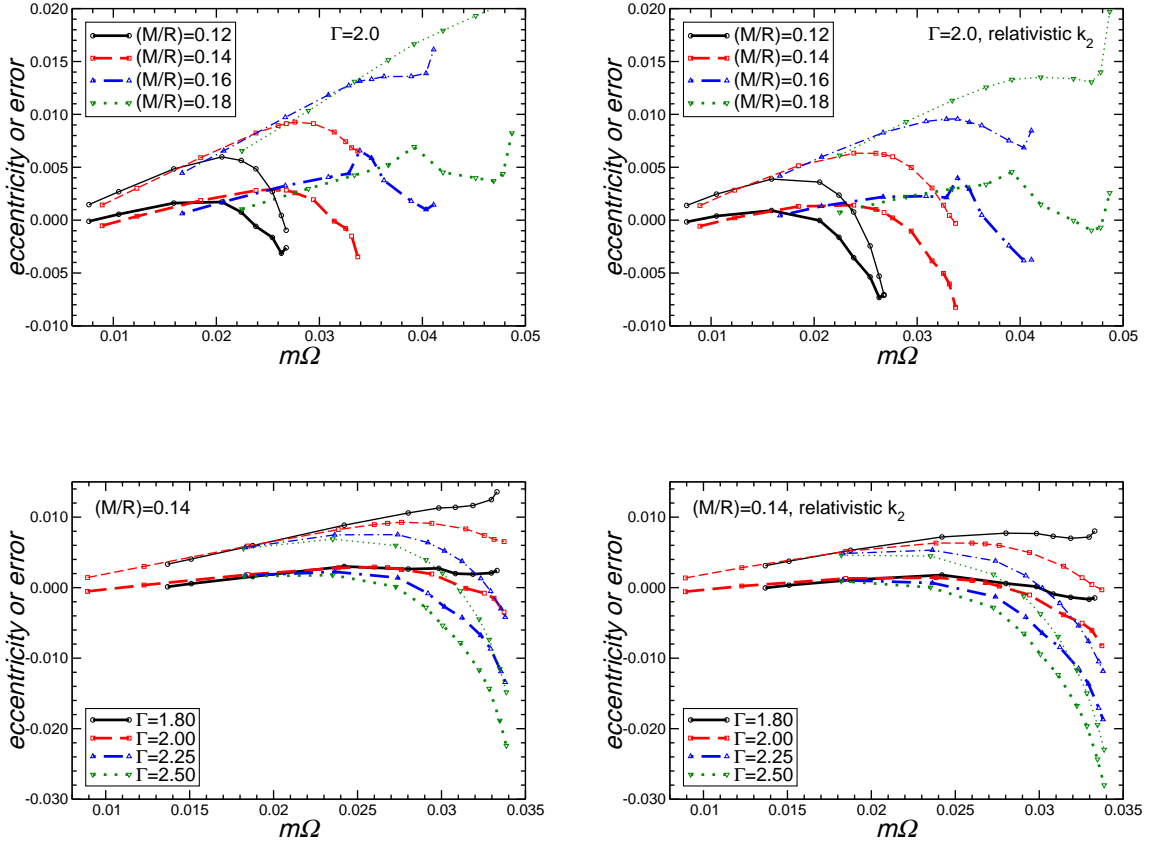


FIG. 1: Best-fit eccentricity estimated from the energy (thick lines) and the angular momentum (thin lines) for irrotational, equal-mass neutron star-neutron star binaries. Top: we fix  $\Gamma = 2.00$  and consider different values of the compactness. Bottom: we fix  $M/R = 0.14$  and consider different values of  $\Gamma$ . Results on the left use the Newtonian apsidal constants, results on the right use the “relativistically corrected” apsidal constants of Eq. (A6).

In comparing with the non-spinning NS-NS initial data sets of [14, 15, 16], our main results can be summarized using Fig. 1. These figures show the eccentricity required to match PN theory with the numerical data for equal-mass systems, for both binding energy (thick lines) and angular momentum (thin lines), for various equations of state, as represented by the adiabatic index  $\Gamma$ , and for various values of the neutron star compactness  $M/R$ . The panels on the left use values for the apsidal constants  $k_2$  and  $k_3$  calculated using Newtonian theory, while those on the right

use values for the dominant  $k_2$  apsidal constant estimated from rotating relativistic stellar models (see Appendix A). The figures are plotted against  $m\Omega$ , where  $m$  is the total gravitational mass of the two isolated stars and  $\Omega$  is the orbital angular velocity. The left-hand end of each plot corresponds to the “Newtonian” limit, where the stars are farther apart; on the right-hand end, the sequences terminate when the stars are within 25 to 40 percent of touching, where cusps in the surface shape are beginning to develop, signalling the onset of mass shedding.

As discussed below (Sec. II), the inferred eccentricity is also an approximate measure of the fractional difference between the data and PN theory assuming circular orbits, so the figures can equally well be interpreted as a measure of the accuracy of the PN-numerical comparison.

From these figures, together with considerations in following sections, we summarize our main results.

*PN theory gives an excellent fit, better than half a percent in most cases, to the binding energy of the numerically generated initial data sequences for all but the closest separations.* Tidal effects matter, and one must use the correct compactness factor and apsidal constants corresponding to the isolated stars and equations of state used in the numerical solutions.

*If circular orbits are assumed, there are systematic differences between the numerical data and the PN diagnostic.* These could be interpreted as being the result of residual eccentricity in the simulations, albeit at levels smaller than those inferred from the BH-BH models in [5, 7]. The differences are larger than can be accounted for either by truncation errors in the PN series or by numerical errors in the initial data sets.

*When best-fit eccentricities are calculated, the values inferred from the energy diagnostic are generally smaller than those inferred from the angular momentum diagnostic.* The same phenomenon was seen in the BH-BH diagnostics [5, 7]. One possibility is that there are poorly understood systematic effects in calculating total angular momentum from numerical initial data sets, or in fixing the intrinsic angular momenta of the individual stars to the desired values (zero in this case).

*A comparison with preliminary initial data for neutron star-black hole binaries shows that the required eccentricities are larger than for NS-NS binaries.* Furthermore, they increase with the mass ratio  $m_{\text{BH}}/m_{\text{NS}}$ . However, because these are early days for NS-BH simulations, the numerical errors in the models are larger than in the more mature NS-NS simulations, so these conclusions should be regarded as tentative. Our PN diagnostic could be a useful tool in helping to refine and improve these initial data sets.

Because tidal effects fall off rapidly with distance and scale with the size of the bodies, the Newtonian tidal contributions are already small, and thus we have argued that post-Newtonian tidal effects are not needed. However, because the neutron stars are highly relativistic, one might question the use of apsidal constants derived from Newtonian theory. We have addressed this by constructing models of isolated, slowly rotating, fully relativistic neutron stars, and by using the rotationally induced deformation to estimate the “relativistic” apsidal constant  $k_2$ . The resulting values can vary by a factor of two over the range of compactness factors considered, leading to small but noticeable effects in the inferred eccentricities (right-hand panels of Fig. 1).

The remainder of this paper provides details. In Sec. II we summarize the post-Newtonian diagnostic equations derived in [6], applicable to both NS-NS and NS-BH non-spinning binaries. In Sec. III we consider the catalogue of quasiequilibrium NS-NS sequences computed by the Meudon group [14, 15, 16]. Section IV considers NS-BH binaries obtained by Taniguchi *et al.* [17, 18, 19] and Grandclément [20]. Section V presents concluding remarks. Appendix A provides details of the calculation of relativistic corrections to the energy, angular momentum and quadrupole moment of rotating isolated neutron stars described by a polytropic equation of state. These calculations were performed using the Hartle-Thorne slow-rotation code described in [21], and are used to estimate “relativistically corrected” values of the apsidal constant  $k_2$ . Hereafter, we use units in which  $G = c = 1$ .

## II. EQUATIONS OF THE PN DIAGNOSTIC

We consider a binary system of bodies of mass  $m_1$  and  $m_2$ , where these masses denote the total, or gravitational mass of an isolated, non-rotating body of given baryon number and equation of state. For black holes, the masses denote irreducible mass. We also define the total mass,  $m \equiv m_1 + m_2$ , and the reduced mass,  $\mu \equiv m_1 m_2 / m$ , along with  $\eta \equiv \mu/m = m_1 m_2 / m^2$  ( $0 < \eta \leq 1/4$ ). We define two quantities  $e$  and  $\zeta$ , related to the eccentricity and semi-latus rectum of the orbit, according to:

$$e \equiv \frac{\sqrt{\Omega_p} - \sqrt{\Omega_a}}{\sqrt{\Omega_p} + \sqrt{\Omega_a}},$$

$$\zeta \equiv \frac{m}{p} \equiv \left( \frac{\sqrt{m\Omega_p} + \sqrt{m\Omega_a}}{2} \right)^{4/3}, \quad (2.1)$$

where  $\Omega_p$  is the value of the orbital frequency  $\Omega$  where it passes through a local maximum (pericenter), and  $\Omega_a$  is the value of  $\Omega$  where it passes through the *next* local minimum (apocenter). These definitions are discussed and justified in [5, 6]; in the Newtonian limit, they agree exactly with the standard definitions. It follows from Eqs. (2.1) that  $\zeta$  also has the property that

$$\zeta = \left( \frac{m\Omega_p}{(1+e)^2} \right)^{2/3} = \left( \frac{m\Omega_a}{(1-e)^2} \right)^{2/3}. \quad (2.2)$$

The diagnostic was restricted to systems of possibly rotating bodies with spin axes aligned perpendicular to the orbital plane (see [6], Eqs. (2.35), (3.6), (3.7), (3.15) and (3.17) for the complete set of ingredients). However, because we will be considering numerical initial data sets for systems with nonrotating bodies, the formulae simplify significantly, because there will be no contributions from rotational kinetic energy or angular momentum, spin-orbit or spin-spin coupling, effects due to rotational distortions or tidal-rotational coupling, and so on. As a result, the total binding energy  $E$  and total angular momentum  $J$  of the system can be written

$$\begin{aligned} E &= E_{\text{Harm}} + E_{\text{Tidal}}, \\ J &= J_{\text{Harm}} + J_{\text{Tidal}}. \end{aligned} \quad (2.3)$$

where the “point-mass” contributions to  $E$  and  $J$ , accurate to third post-Newtonian (3PN) order, and expressed in harmonic coordinates, are given by (recall that  $\zeta \sim O(\epsilon)$ )

$$\begin{aligned} E_{\text{Harm}} &= -\frac{1}{2}m\eta(1-e^2)\zeta \left\{ 1 - \left[ \frac{3}{4} + \frac{1}{12}\eta - \left( \frac{1}{12} - \frac{1}{4}\eta \right) e^2 \right] \zeta \right. \\ &\quad - \left[ \frac{27}{8} - \frac{19}{8}\eta + \frac{1}{24}\eta^2 - \left( \frac{17}{12} + 4\eta + \frac{1}{4}\eta^2 \right) e^2 + \left( \frac{1}{24} + \frac{29}{24}\eta - \frac{1}{8}\eta^2 \right) e^4 \right] \zeta^2 \\ &\quad - \left[ \frac{675}{64} - \left( \frac{34445}{576} - \frac{205}{96}\pi^2 \right) \eta + \frac{155}{96}\eta^2 + \frac{35}{5184}\eta^3 \right. \\ &\quad + \left( \frac{7}{64} - \left( \frac{2369}{576} + \frac{41}{96}\pi^2 \right) \eta + \frac{11951}{864}\eta^2 - \frac{25}{576}\eta^3 \right) e^2 \\ &\quad - \left( \frac{815}{576} - \frac{7619}{1728}\eta - \frac{1499}{288}\eta^2 - \frac{25}{64}\eta^3 \right) e^4 \\ &\quad \left. \left. - \left( \frac{35}{5184} - \frac{143}{192}\eta + \frac{57}{32}\eta^2 - \frac{5}{64}\eta^3 \right) e^6 \right] \zeta^3 \right\}, \end{aligned} \quad (2.4a)$$

$$\begin{aligned} J_{\text{Harm}} &= \frac{m^2\eta}{\sqrt{\zeta}} \left\{ 1 + \left[ \frac{3}{2} + \frac{1}{6}\eta - \left( \frac{1}{6} - \frac{1}{2}\eta \right) e^2 \right] \zeta \right. \\ &\quad + \left[ \frac{27}{8} - \frac{19}{8}\eta + \frac{1}{24}\eta^2 + \left( \frac{23}{12} - \frac{31}{6}\eta - \frac{1}{4}\eta^2 \right) e^2 + \left( \frac{1}{24} - \frac{35}{24}\eta - \frac{1}{8}\eta^2 \right) e^4 \right] \zeta^2 \\ &\quad + \left[ \frac{135}{16} - \left( \frac{6889}{144} - \frac{41}{24}\pi^2 \right) \eta + \frac{31}{24}\eta^2 + \frac{7}{1296}\eta^3 \right. \\ &\quad + \left( \frac{299}{16} - \left( \frac{10003}{144} - \frac{41}{24}\pi^2 \right) \eta + \frac{3013}{216}\eta^2 - \frac{5}{144}\eta^3 \right) e^2 \\ &\quad + \left( \frac{77}{144} - \frac{6497}{432}\eta + \frac{853}{72}\eta^2 + \frac{5}{16}\eta^3 \right) e^4 \\ &\quad \left. \left. - \left( \frac{7}{1296} + \frac{1}{16}\eta + \frac{1}{8}\eta^2 - \frac{1}{16}\eta^3 \right) e^6 \right] \zeta^3 \right\}. \end{aligned} \quad (2.4b)$$

Expressions for  $E$  and  $J$  are also available in Arnowitt-Deser-Misner (ADM) coordinates [6]; however the differences are negligible for the systems in question. The tidal contributions to  $E$  and  $J$  are given by,

$$E_{\text{Tidal}} = m\eta(1-e^2) \left[ \frac{1}{18}(9+10e^2-3e^4)B\zeta^6 + \frac{1}{24}(13+49e^2+7e^4-5e^6)C\zeta^8 \right], \quad (2.5a)$$

$$J_{\text{Tidal}} = m^2\eta \left[ \frac{2}{9}(3+10e^2+3e^4)B\zeta^{9/2} + \frac{2}{3}(1+7e^2+7e^4+e^6)C\zeta^{13/2} \right], \quad (2.5b)$$

where

$$\begin{aligned} B &= 6\eta \left[ q_1^5 k_2^{(1)} \left( \frac{m_1}{m} \right)^3 + q_2^5 k_2^{(2)} \left( \frac{m_2}{m} \right)^3 \right], \\ C &= 8\eta \left[ q_1^7 k_3^{(1)} \left( \frac{m_1}{m} \right)^5 + q_2^7 k_3^{(2)} \left( \frac{m_2}{m} \right)^5 \right]. \end{aligned} \quad (2.6)$$

For each body,  $q_a \equiv R_a/m_a$  is the inverse of the “compactness parameter”, where  $R_a$  is its radius in harmonic coordinates, and  $k_2^{(a)}$  and  $k_3^{(a)}$  denote the “apsidal constants” for angular harmonics  $l = 2$  and  $l = 3$ , respectively (higher harmonics make negligible contributions). In Newtonian gravity, the apsidal constants depend only on the harmonic index  $l$  and on the equation of state; their values are shown in Appendix A, Table III. Notice that the leading contribution to the tidal terms is of order  $\zeta^5$  relative to the Newtonian contributions to  $E$  or  $J$ , or effectively 5PN order. This is why a Newtonian treatment of tides is justified. We also note that, in calculating  $E/m$  and  $J/m^2$ , only mass ratios are relevant, since, apart from the dependence on  $\zeta$ , the expressions depend only on  $\eta$ ,  $m_1/m$  or  $m_2/m$ .

In comparing this analytical diagnostic with numerical initial data, one must carefully translate the meaning of the variables in the two approaches. The PN masses  $m_a$  are the physically measured masses of the corresponding isolated body; these correspond directly to the ADM masses of the isolated bodies defined in numerical relativity. Similarly, numerical stellar radii are generally computed in ADM coordinates, which, for an isolated body corresponds to the isotropic radial coordinate of the Schwarzschild geometry; we denote this radius by  $R_{ADM}$ . Alternatively, one could compute, from the numerical data, the proper circumferential or areal radius of the isolated star  $[\mathcal{C}/2\pi$  or  $(\mathcal{A}/4\pi)^{1/2}$ ], which would correspond to the Schwarzschild radial coordinate  $R_S$ . The relationship between the PN harmonic radial coordinate  $R_H$  and the others is

$$R_H = R_S - M_{ADM} = R_{ADM} \left( 1 + \frac{M_{ADM}^2}{4R_{ADM}^2} \right). \quad (2.7)$$

Since for neutron stars,  $M_{ADM}/R_{ADM} < 0.2$ , the difference between  $R_H$  and  $R_{ADM}$  is generally less than one percent, and is thus negligible for our purposes. For non-rotating black holes, the relevant radius is  $R_H = m_{BH}$ , but since tidal effects are negligible for the separations to be considered, this will not play a role.

Finally, we note that, inserting Eq. (2.2) into the Newtonian part of Eqs. (2.4), we obtain to leading order,

$$\begin{aligned} E/m &\approx -\frac{1}{2}\eta(m\Omega)^{2/3} \left[ 1 + \frac{4}{3}e + O(e^2) \right] + O[(m\Omega)^{4/3}], \\ J/m^2 &\approx \eta(m\Omega)^{-1/3} \left[ 1 - \frac{2}{3}e + O(e^2) \right] + O[(m\Omega)^{1/3}]. \end{aligned} \quad (2.8)$$

Thus, apart from factors of  $4/3$  or  $2/3$ , the eccentricity  $e$  can be viewed as a measure of the fractional deviation of the energy and angular momentum from its circular orbit value for a given  $m\Omega$ . If the inferred value of  $e$  is positive, the binary system is at apocenter; if the inferred value is negative, it really corresponds to a positive eccentricity, but with the binary system at pericenter.

### III. QUASIEQUILIBRIUM BINARY NEUTRON STAR INITIAL CONFIGURATIONS

#### A. Numerical Calculations

The first numerical calculations of initial data for binary neutron stars in full general relativity were carried out, for the case of momentarily corotating bodies, by Baumgarte *et al.* [25, 26] and Marronetti *et al.* [27]. Miller *et al.* [13] performed convergence tests and included error bars in their simulations of corotating neutron stars.

The first results for the more physically realistic case of non-spinning, or irrotational binary neutron stars were presented by the Meudon group using spectral methods [14, 28], by Marronetti *et al.* using a single-domain finite difference method in Cartesian coordinates [29], and by Uryu *et al.* using quasispherical coordinates [30, 31, 32]. Generalization to other values of the stellar rotation rates was carried out in [33].

We will focus on simulations of non-spinning binary neutron stars by the Meudon group in [14, 15, 16]. They assume that the system is in a *quasiequilibrium* state, meaning that, in a reference frame that momentarily rotates with the orbital angular velocity, the system is stationary (technically implying the existence of a “helical Killing vector”  $\partial/\partial t + \Omega\partial/\partial\phi$ ). They assume that the fluid flow is irrotational with respect to the global frame and that the

induced spatial metric is conformally flat. They use a multidomain spectral method with two patches of surface-fitting coordinates, to solve for the five metric functions (lapse, conformal factor and shift 3-vector) and the velocity potential of the fluid. The input information is an equation of state of each star; an initial coordinate separation  $d$ ; and the central enthalpy (or density) of each star, or alternatively the baryonic mass of each star.

The equation of state used is a zero-temperature polytrope with  $p = \kappa \rho^\Gamma$ , where where  $p$  and  $\rho$  are the pressure and mass density, and  $\Gamma$  is the adiabatic index. Such equations of state are also parametrized by a “polytropic index”  $n$ , related to  $\Gamma$  by  $\Gamma = 1 + 1/n$ . Most groups use “polytropic” units, whereby one defines a length scale

$$R_{\text{poly}} = \kappa^{1/[2(\Gamma-1)]}, \quad (3.1)$$

and rescales every quantity by  $R_{\text{poly}}$  to make it dimensionless. With this choice, equilibrium models are characterized only by  $\Gamma$  and by the (dimensionless) central energy density of each body (see eg. Sec. 2.6.1 of [34] for a detailed explanation of these units).

In Ref. [14] calculations were limited to binaries of equal mass and to a single polytropic EOS with  $\Gamma = 2$ ,  $M/R = 0.14$  and baryonic mass  $M_B = 1.625 M_\odot$ . Results were given in their Table III. Taniguchi and Gourgoulhon [15], again with  $\Gamma = 2$ , extended the calculations to corotating and non-spinning binaries of varying compactness, and also with unequal masses. Finally in Ref. [16] calculations were presented for an extensive sample of values of  $\Gamma$  and of  $M/R$ , for both equal and unequal masses. Comparison of the endpoints of their sequences of models with those of Uryu *et al.* [30, 31, 32] showed good agreement [16]. Our Tables I and II summarize schematically the different quasiequilibrium sequences considered by the Meudon group, pointing to the relevant Tables in the original papers [15, 16].

TABLE I: Filled entries mark combinations of  $\Gamma = 1 + 1/n$  and  $M/R$  considered by the Meudon group for equal-mass binaries. For non-spinning configurations, bullets mark cases for which we plotted  $E/m$  and  $J/m^2$ , and circles mark cases for which we plotted the inferred eccentricities. The third and fourth columns give the maximum baryonic mass  $M_B^{\text{max}}$  and maximum compactness  $(M/R)^{\text{max}}$ , respectively, for the given polytropic model. “Cor” means corotating stars, “NoS” means non-spinning stars. The last three columns give the Tables and References where the corresponding numerical data are tabulated.

Parameters				$M/R$							Table		Ref.
$\Gamma$	$n$	$M_B^{\text{max}}$	$(M/R)^{\text{max}}$	0.08	0.10	0.12	0.14	0.16	0.18	0.20	Cor	NoS	
1.80	5/4	0.217	0.172	•	×	×	•○				X	XII	[16]
2.00	1	0.180	0.214			•○	○	○	•○		I	III	[15]
2.25	4/5	0.162	0.252			×	○	×	×		VI	VIII	[16]
2.50	2/3	0.155	0.278				•○	×	×	•	II	IV	[16]

TABLE II: Same as Table I, but for unequal-mass binaries.

Parameters		$(M/R)_1 + (M/R)_2$						Table		Ref.
$\Gamma$	$n$	(0.08 + 0.10)	(0.10 + 0.12)	(0.12 + 0.14)	(0.14 + 0.16)	(0.16 + 0.18)	(0.18 + 0.20)	Cor	NoS	
1.80	5/4	×	×	×				XI	XIII	[16]
2.00	1			•	×	•		II	IV	[15]
2.25	4/5			×	×	×		VII	IX	[16]
2.50	2/3				×	×	×	III	V	[16]

## B. PN diagnosis of Meudon data

The tables of Refs. [14, 15, 16] display the total ADM mass  $\bar{M}$ , angular momentum  $\bar{J}$  and angular velocity  $\bar{\Omega}$  of the system (among other variables) for the various models. Overbars denote that all variables are in polytropic units. One piece of information missing from those tables is the ADM mass of each star in isolation; these values were kindly provided to us by Keisuke Taniguchi, along with tables of all data that went into those references, but with full untruncated precision.

It is then straightforward to compute  $E/m$  and  $J/m^2$  using Eqs. (2.3) – (2.6) as functions of  $m\Omega$ , for each value of  $\Gamma$  (which determines the apsidal constants) and the compactness parameter, together with the provisional assumption

that  $e = 0$ . From the numerical data the corresponding binding energy and angular momentum are given by

$$\begin{aligned} \left(\frac{E}{m}\right)_{\text{Num}} &= \frac{\bar{M}}{\bar{M}_{\text{ADM},0}} - 1, \\ \left(\frac{J}{m^2}\right)_{\text{Num}} &= \frac{\bar{J}}{\bar{M}_{\text{ADM},0}^2}, \\ (m\Omega)_{\text{Num}} &= \bar{M}_{\text{ADM},0} \bar{\Omega}, \end{aligned} \quad (3.2)$$

where  $\bar{M}_{\text{ADM},0}$  is the sum of the ADM masses of the two stars in isolation. We then plot  $(E/m)_{\text{Num}}$  and  $(J/m^2)_{\text{Num}}$  against  $(m\Omega)_{\text{Num}}$ . Since the final quantities  $E/m$ ,  $J/m^2$  and  $m\Omega$  are dimensionless, the polytropic units scale out. The compactness parameter is quoted as  $(M/R)$ , where here  $M$  is the ADM mass of the isolated star, and  $R$  is the areal, or Schwarzschild radius (the value is independent of whether polytropic or normal units are used); as a result, using Eq. (2.7), we can read off the value

$$(q)_{\text{Num}} = \left(\frac{R}{M}\right) - 1. \quad (3.3)$$

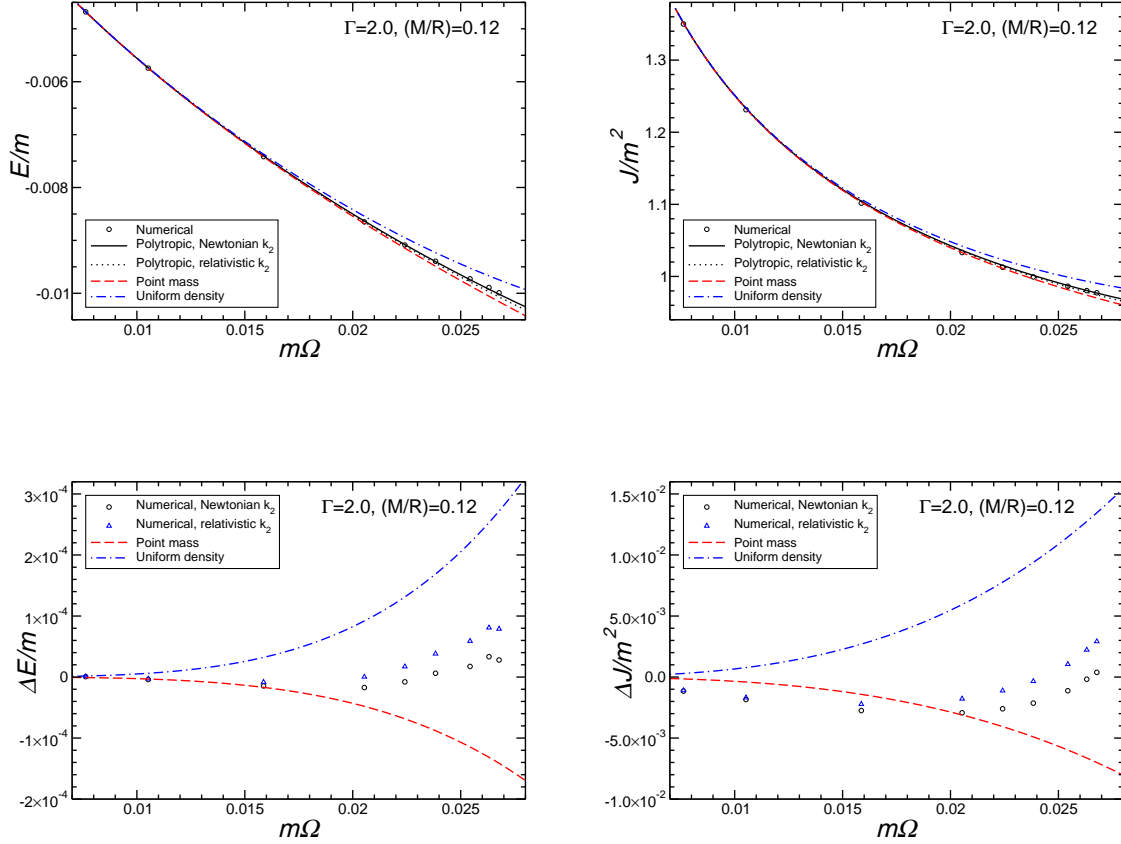


FIG. 2: Binding energy and angular momentum vs.  $m\Omega$  for equal masses,  $\Gamma = 2.0$ ,  $(M/R)_1 = (M/R)_2 = 0.12$ . Top: circles are the numerical data points, solid (black) line is the PN diagnostic using the Newtonian apsidal constant values (Table III) for  $\Gamma = 2$ , dashed (red) line has no tidal contributions; dot-dashed (blue) line uses the uniform density values for the apsidal constants; dotted (black) line uses the “relativistically corrected” apsidal constants of Eq. (A6). Bottom: Numerical data (circles), point-mass (dashed-red) and uniform-density (dot-dashed-blue) plotted relative to  $\Gamma = 2$  PN diagnostic as the baseline. Triangles denote numerical data plotted relative to  $\Gamma = 2$  PN diagnostic using the relativistically corrected apsidal constants.

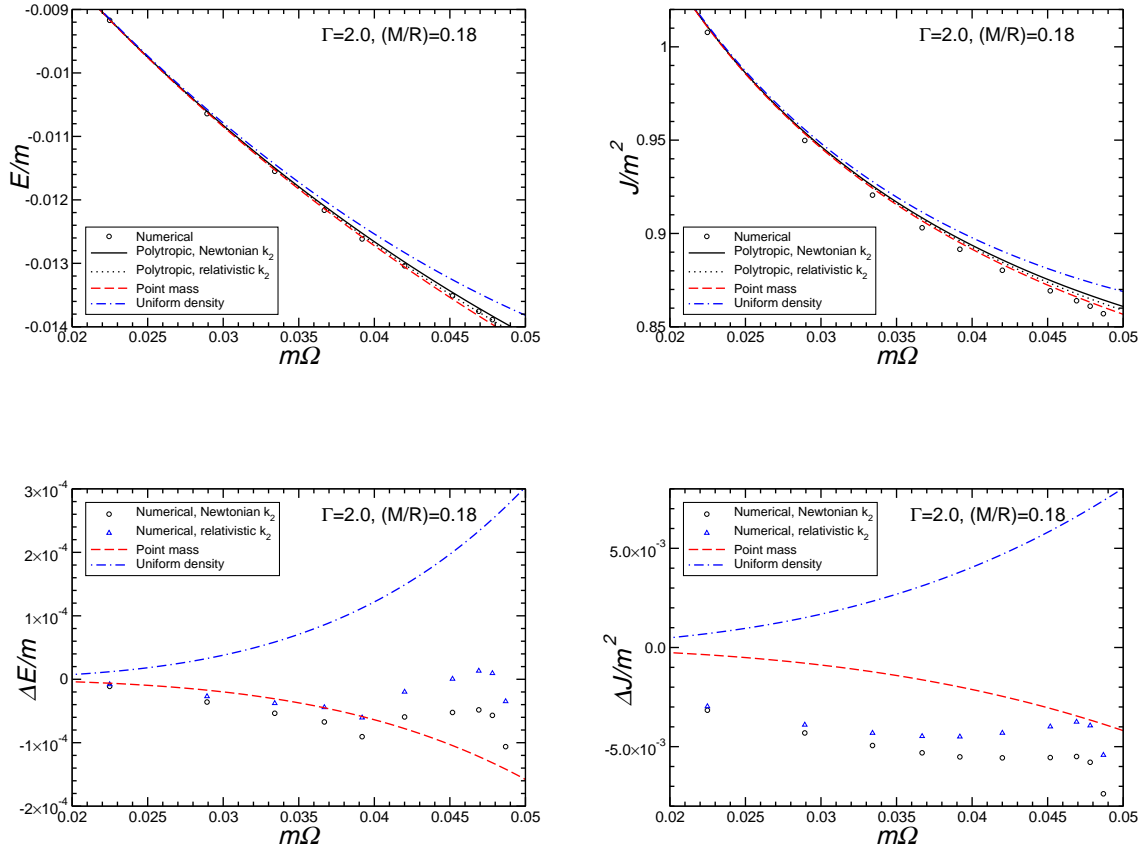


FIG. 3: Same as Fig. 2, for  $\Gamma = 2.0$ ,  $(M/R)_1 = (M/R)_2 = 0.18$ .

Figures 2 and 3 show the results for equal masses,  $\Gamma = 2$  and compactness values 0.12 and 0.18, corresponding respectively to neutron star harmonic radii 7.3 and 4.5 in units of the stellar mass. The top figures show, on a gross scale, the overall agreement between the PN and numerical results. Using differences between data sets, the bottom figures magnify the scale: the circles and triangles show the difference between the numerical data and our diagnostic using the Newtonian and relativistically corrected apsidal constants respectively. The dashed and dot-dashed curves illustrate the importance of taking tidal effects into account; respectively, they show the difference between the PN values for energy and angular momentum assuming the Newtonian apsidal constants and those assuming point masses (no tidal effects) or those assuming uniform density bodies (maximum tidal effects). It is clear that the numerical data agree much better with PN formulae that include appropriate tidal effects than they do with formulae that assume either point masses or homogeneous bodies. The agreement is at the level of a percent or better over the range of  $m\Omega$  shown. However, as in the binary BH case, there appears to be a systematic offset between the data and the diagnostic for  $J/m^2$ . We note that the use of a relativistically corrected apsidal constant (triangles) has a small effect on the agreement. As discussed in Appendix A, relativistic effects tend to decrease the apsidal constant  $k_2$ ; this has the effect of raising the data points on the difference plots compared to the Newtonian diagnostic baseline.

Figure 4 shows differences relative to the PN diagnostic baseline for other values of  $\Gamma$  and  $M/R$  for equal masses. The agreement between diagnostic and data seems to worsen as the EOS progress from soft to hard and the compactness increases; again there is a systematic offset in  $J/m^2$ , even in the non-relativistic limit. Figure 5 shows differences for selected configurations of unequal-mass neutron stars.

Instead of comparing the data with a circular-orbit diagnostic, we now let the eccentricity be a free parameter, and find the value of  $e$  that gives the best fit to the data. Using both the Newtonian and the relativistic apsidal constants, we show the results for a range of EOS and compactness parameters in Fig. 1. We note that the inferred eccentricities are generally smaller than those inferred from the binary BH initial data, and that there is again a difference between



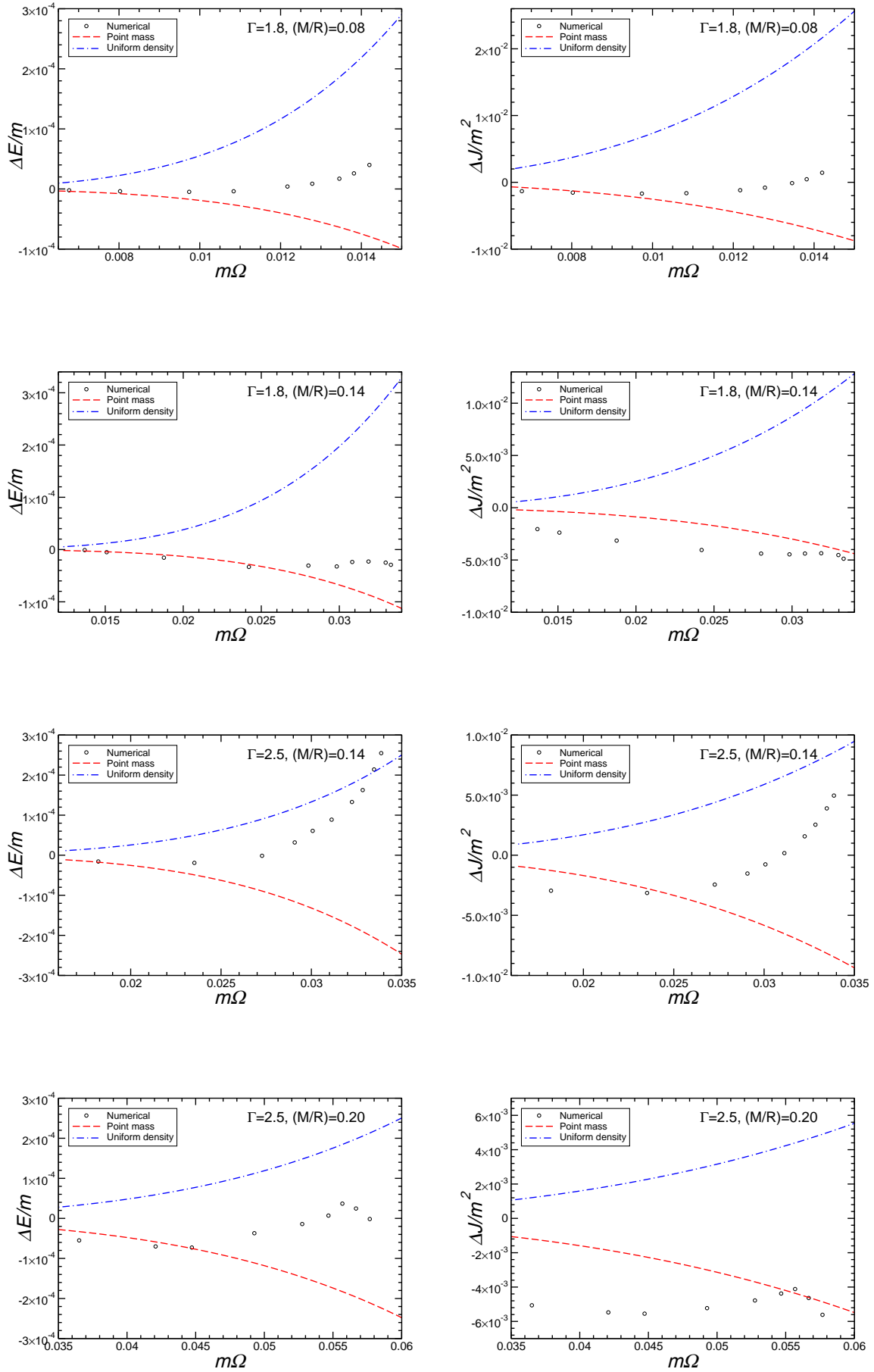


FIG. 4: Same as the bottom panels of Fig 2, for various values of  $\Gamma$  and  $M/R$ , for equal mass binaries.

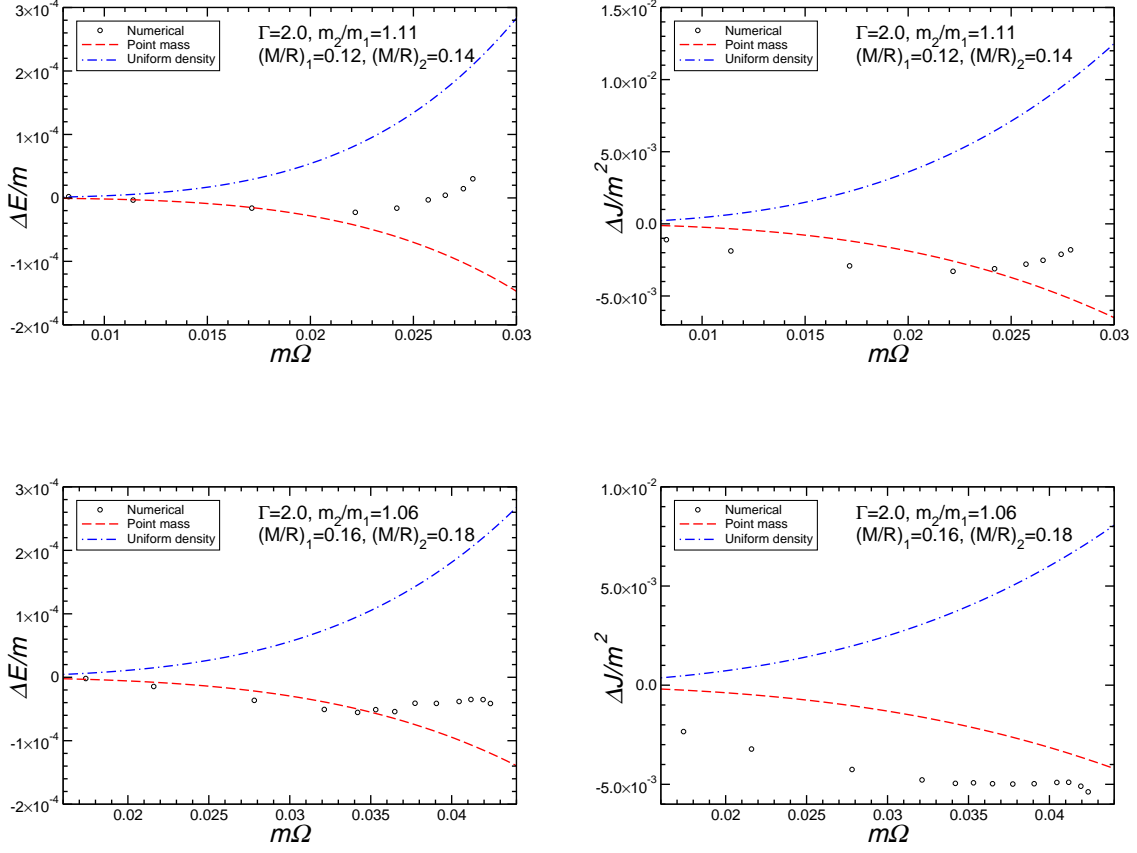


FIG. 5: Same as Fig. 4, but for binaries with different masses.

the values inferred from angular momentum and those inferred from energy. The energy-inferred eccentricities are generally less than 0.005 for all but the high-frequency ends of each quasiequilibrium sequence. The end points of these sequences correspond to binary separations only 25 to 40 percent larger than the sum of the stellar radii; at these separations, tidal effects are sufficiently strong that cusps in the surface shape of the stars are about to form, signalling the onset of mass shedding. Not only is our simple tidal model likely to be inadequate, but also there are larger errors in the numerical data near these end points (see [18] for discussion).

The inferred eccentricities are very small, and it is worth asking how significant they are, given that the PN approximation used in our diagnostic has truncation errors, and that the numerical simulations have numerical errors. Figure 6 is an attempt to quantify this. We plot the energy-inferred eccentricities for two representative models, with  $\Gamma = 2$ ,  $(M/R) = 0.12$ , and  $\Gamma = 2.5$ ,  $(M/R) = 0.14$ . The solid curve is ten times what one would crudely estimate for the 4PN contributions to the energy for equal masses, or  $10 \times \zeta^5/8 = 1.25(m\Omega)^{10/3}$ , while the dotted curves are  $(3/64)q^5 k_2 (m\Omega)^{14/3}$  for the two corresponding values of  $q$  and  $k_2$ , which represent a post-Newtonian-tidal correction, or  $\zeta$  times the leading tidal term in Eq. (2.5a). Also plotted as dashed curves with data points are the corresponding “virial” errors  $VE(M)$ , computed from the numerical data, and tabulated in [15, 16], where  $VE(M) \equiv |M_{\text{ADM}} - M_{\text{Komar}}|/M_{\text{ADM}}$ , where  $M_{\text{Komar}}$  is a certain global integral known as the Komar mass. This and similar virial theorems are one indication of the accuracy of the numerical solution. We see that PN truncation errors are smaller by an order of magnitude than the inferred eccentricities or “errors” from the diagnostic, and that the numerical errors are generally smaller, except in the extreme Newtonian limit. This gives some confidence that our PN diagnostic can in many cases “diagnose” real physics in the numerical simulations.

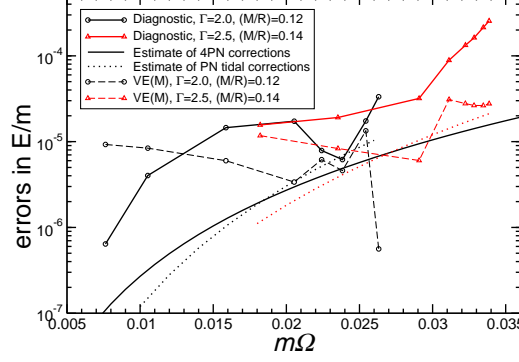


FIG. 6: Comparison of PN diagnostic eccentricities or errors with truncation errors in the PN approximation and with “virial” errors in the numerical simulations.

#### IV. QUASIEQUILIBRIUM CALCULATIONS OF NEUTRON STAR-BLACK HOLE SYSTEMS

The first numerical calculations of fully relativistic neutron star-black hole binaries were carried out by the Illinois group, for corotating stars, and in the limit where the black hole was 10 times more massive than the neutron star [35]. However, following a number of technical improvements, the group recently presented results for quasiequilibrium sequences of non-spinning NS-BH binaries with a range of five mass ratios (including equal masses), and two values of the compactness parameter of the neutron star [17, 18]. They assume a conformally flat spatial metric and solve the initial value equations for the metric variables using multidomain spectral methods. Since then, they have also implemented a more accurate condition for ensuring that the black hole is nonspinning, first introduced in Ref. [36]. Taniguchi has provided us with preliminary data for the improved sequences [19]. Using similar methods, Grandclément [20] also obtained quasiequilibrium NS-BH sequences, for a mass ratio of five and for four values of the compactness parameter. To date, all NS-BH calculations have assumed  $\Gamma = 2$ .

As in the NS-NS case, results are given in polytropic units, with  $E/m$ ,  $J/m^2$  and  $m\Omega$  already tabulated as in Eq. (3.2) along with the mass ratio  $M_{\text{BH}}^{\text{BH}}/M_{\text{ADM},0}^{\text{NS}}$  and the ADM mass  $\bar{M}_{\text{ADM},0}^{\text{NS}}$  and compactness parameter  $M_{\text{ADM},0}^{\text{NS}}/R_0$  of the isolated neutron star, where  $R_0$  is again the areal radius. From these data, we compute the factor  $q$  for the neutron star from  $q = R_0/M_{\text{ADM},0}^{\text{NS}} - 1$ .

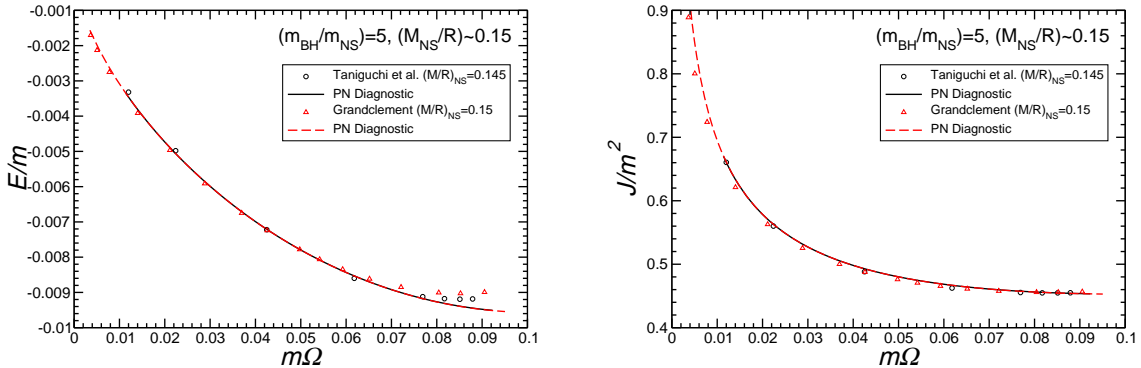


FIG. 7: Binding energy and angular momentum vs.  $m\Omega$  for a black hole-neutron star binary with mass ratio 5. Plotted are data from Taniguchi *et al.* (circles) and from Grandclément (triangles), along with the corresponding PN diagnostic curve for circular orbits.

Figure 7 shows the gross agreement between the Taniguchi *et al.* and Grandclément data, for the one case (mass ratio

5, compactness  $\sim 0.15$ ) where they can be compared, and between the data and the corresponding PN diagnostics. Figure 8 shows the inferred eccentricities (or the accuracies of the PN comparisons) for all the NS-BH data sets. The eccentricities are somewhat larger than in the NS-NS case (and significantly larger for the Grandclément mass ratio 5 : 1 data), and vary more strongly as a function of  $m\Omega$ , especially near the end-points of the sequences, where the larger tidal deformations cause numerical errors. In addition, the eccentricities (or errors) appear to increase with mass ratio. This may not be surprising, as both numerical groups acknowledge that numerical errors tend to increase with mass ratio. At the same time, the convergence of the PN series depends on mass ratio, being best for equal masses, and rather poor for extreme mass ratios (see Fig. 1 of Ref. [6]). In the equal-mass case, where the numerical errors are smallest and the PN series converges the best, the inferred eccentricities are small, less than 0.01 from the energy.

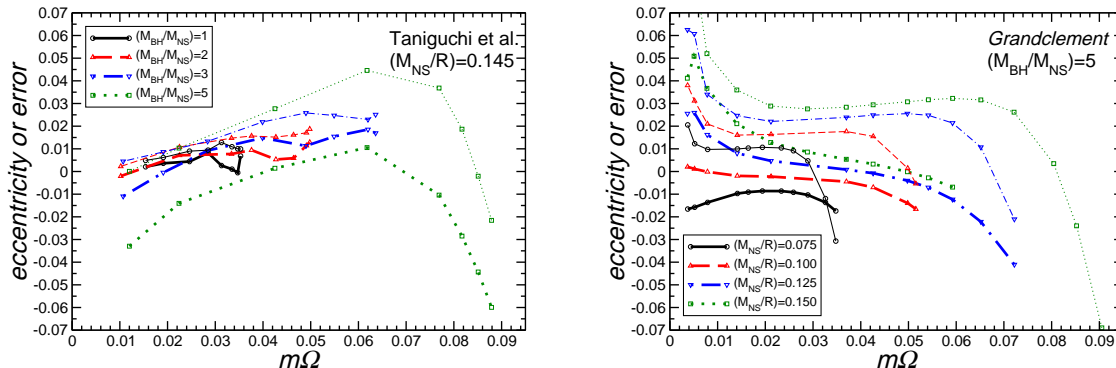


FIG. 8: Best-fit eccentricity estimated from the energy (thick lines) and the angular momentum (thin lines) for irrotational, black hole-neutron star binaries. Left: improved data from Taniguchi *et al.* [19], for a compactness factor of 0.145, and four mass ratios. Right: data from Grandclément, for a single mass ratio of 5:1, and a range of compactness factors. The dotted curves in each figure correspond to a mass ratio 5 and similar compactness factors; they also correspond to the data plotted in Fig. 7.

Because these NS-BH numerical simulations are still in their infancy compared to the BH-BH and NS-NS simulations, it is premature to draw definite conclusions from comparisons with PN theory. Instead, a PN diagnostic may be a useful tool in testing improved simulations. For example, in comparing eccentricities inferred from the original data published in [18] with those inferred from the unpublished data [19] that used an improved black-hole zero spin condition (plotted in the left panel of Fig. 8) we found a significant reduction in the disagreement between values of  $e$  inferred from  $E$  and those inferred from  $J$ , especially at the closer separations. In Fig. 8 (left panel) the eccentricities from  $E$  and  $J$  closely track each other for the mass ratios 1, 2 and 3, both increasing slightly with  $m\Omega$ ; with the earlier data, the eccentricities inferred from  $J$  actually grew strongly with  $m\Omega$ , diverging from those inferred from  $E$ . A similar improvement resulting from the new black-hole spin condition was noted in BH-BH simulations (see [7], Fig. 2).

## V. CONCLUSIONS

We have used a post-Newtonian diagnostic tool to examine initial data sets for non-spinning, double neutron star and neutron star-black hole binary systems. The PN equations included the effects of tidal interactions, parametrized by the compactness of the neutron stars and by suitable values of apsidal constants.

We found that PN theory agrees quite well with the NS-NS initial data, typically to better than half a percent except where tidal distortions are becoming extreme. The differences between PN theory and the numerics are sufficiently large and systematic that they could be interpreted as representing residual eccentricity in the initial orbits. It will be interesting to see if simulations of the time-evolution from these initial data sets show signs of eccentricity in the orbits.

Comparison of our PN diagnostic with NS-BH initial data sets showed poorer agreement, not inconsistent with the larger numerical errors present in these preliminary results. We argued that a PN diagnostic could be a useful tool for examining future improved data for NS-BH binaries.

Tidal effects depend on the values of the apsidal constants, and we addressed how relativistic neutron-star structure would affect their values. An open question is whether our estimate of a relativistic  $k_2$  from rotational deformations is a reasonable estimate of the tidally-induced  $k_2$ . This would be an interesting and important problem in relativistic stellar structure.

### Acknowledgments

We thank Greg Cook, Eric Gourgoulhon, Philippe Grandclément, Mark Miller, Wai-Mo Suen and Keisuke Taniguchi for useful discussions and for sharing with us their numerical data. This work was partially funded by the National Science Foundation under grant numbers PHY 03-53180 and PHY 06-52448. CMW and EB are grateful to the Institut d’Astrophysique de Paris, Université Pierre et Marie Curie for their hospitality during the final stages of this work.

## APPENDIX A: TIDAL EFFECTS IN RELATIVISTIC NEUTRON STARS

In [6], we argued that, for compact bodies such as neutron stars or black holes, the effects of finite size, such as rotational kinetic energy, tidal distortions, and so on, would be of effectively higher PN order than expected a priori, because the bodies’ sizes scale as their masses  $M$ , i.e.  $R \sim q M$ , where  $q$  is a factor of order unity. Thus, for example, the rotational kinetic energy of a body can be expressed as  $E_{\text{Rot}} \sim I\omega^2/2 \sim MR^2(M/r^3)(\omega/\Omega)^2 \leq E_N q^2 (M/r)^2$ , where  $E_N$  is the Newtonian orbital energy, and  $\omega$  is the body’s rotational angular velocity. For compact bodies that are rotating no faster than the orbital angular velocity, rotational kinetic energy can thus be viewed as an effectively 2PN contribution to the energy, even though formally it is a Newtonian effect.

Similarly, tidal deformations have the dependence  $E_{\text{Tidal}} \sim (M^2/R)(R/r)^6 \sim E_N q^5 (M/r)^5$ , and so are effectively 5PN order. However, for neutron stars,  $q$  can be as large as 8, and so the effects could be important, as we have seen.

While we have argued that the smallness of these effects justifies a Newtonian treatment of tidal and rotational deformations [6], one might worry that, in relativistic neutron stars, the values of such quantities as apsidal constants could differ strongly from their Newtonian values. In this appendix, we address this question.

Unfortunately, it is difficult to treat tidal effects in relativistic stars, because that would involve constructing a relativistic stellar model in the gravitational field of another body, which is exactly the problem of inspiralling binaries treated by numerical relativity.

On the other hand, there is now a rather complete description of isolated rotating relativistic stars. In Newtonian gravity, there is no distinction between rotational flattening and tidal distortion, at least for  $l = 2$  linear perturbations, and thus a single apsidal constant  $k_2$  applies to both distortions (the only difference is that one distortion is oblate while the other is prolate). For higher  $l$  this degeneracy breaks down. In relativity, by contrast, there is a difference in principle between rotational and tidal deformation for  $l = 2$ , even for linear perturbations, because of the presence in rotating stars of such phenomena as frame-dragging and the relativistic contributions of rotational kinetic energy to self-gravity. Nevertheless, for the slowly rotating configurations that we expect to be relevant to estimating apsidal constants for small distortions, we might assume that the  $k_2$  that governs rotationally induced distortions in a relativistic star might not be too different from the  $k_2$  that governs tidal distortions. This permits one to read off  $k_2$  from the quadrupole moment induced by the slow rotation.

Because the effects of  $k_3$  were extremely small in our diagnostic, we will not consider this apsidal constant further. Therefore, in this appendix we will endeavor to estimate  $k_2$  for relativistic neutron stars and compare the results with those derived from Newtonian gravity. First we review the calculation of Newtonian apsidal constants.

### 1. Apsidal constants in Newtonian gravity

In Newtonian gravity, apsidal constants can be computed by a standard method for different polytropic indices  $n$  or  $\Gamma = 1 + 1/n$  and different values of  $l$  using the numerical method described in [22]. The results are listed, for example, in the classical monographs by Kopal [23, 24]. Unfortunately these works do not list apsidal constants for  $n = 2/3$ , 0.8 and 1.25. Since these values are needed for neutron stars, we report here results of our own numerical calculations. In Newtonian gravity, apsidal constants are defined by the relation (see Appendix B of [6] for a detailed discussion)

$$k_l = \frac{l+1-\eta_l(R)}{2l+2\eta_l(R)}, \quad (\text{A1})$$

TABLE III: Newtonian apsidal constants (compare with Table II in [22] and Table II in [23]);  $l$  is the angular harmonic index,  $\Gamma$  and  $n$  are adiabatic indices, with  $\Gamma = 1 + 1/n$ .

$l$	$n = 2/3$	$n = 0.80$	$n = 1.00$	$n = 1.25$	$n = 1.50$	$n = 2.00$	$n = 2.50$
	$\Gamma = 2.5$	$\Gamma = 2.25$	$\Gamma = 2$	$\Gamma = 1.8$	$\Gamma = 1.67$	$\Gamma = 1.5$	$\Gamma = 1.4$
2	0.375966	0.325098	0.259909	0.194339	0.143279	0.073938	0.034852
3	0.164696	0.138660	0.106454	0.075590	0.052849	0.024394	0.010192
4	0.098546	0.081155	0.060241	0.040967	0.027393	0.011508	0.004342
5	0.067424	0.054485	0.039293	0.025748	0.016569	0.006420	0.002220
6	0.049791	0.039575	0.027827	0.017651	0.010984	0.003966	0.001272
7	0.038649	0.030270	0.020810	0.012824	0.007745	0.002628	0.000789

where  $R$  is the stellar radius and the function  $\eta_l$  is a solution of the Clairaut-Radau differential equation

$$r\eta'_l + \eta_l(\eta_l - 1) + 6D(\eta_l + 1) = l(l + 1), \quad (\text{A2})$$

with initial condition  $\eta_l(0) = l - 2$ . A prime denotes a derivative with respect to the distance  $r$  from the center of the star; the quantity  $D \equiv \rho(r)/\bar{\rho}(r)$ , where  $\rho(r)$  is the density of the undistorted configuration at  $r$  and  $\bar{\rho}(r)$  is the mean density inside the volume of radius  $r$ . Of course, to obtain the density profile we must specify an equation of state. The simplest choice is a (Newtonian) polytropic EOS  $\rho = \rho_c y^n$ , where  $\rho_c$  is the central density,  $n$  is the polytropic index and  $y$  satisfies the Lane-Emden differential equation

$$y'' + \frac{2}{r}y' + y^n = 0, \quad (\text{A3})$$

subject to the initial conditions  $y(0) = 1$ ,  $y'(0) = 0$ . We integrated the system (A2-A3) following the method described in [22]. Table III shows the results. When a comparison with Table II of [22] is possible, the agreement is usually at the level of five to six decimal places or better.

## 2. Apsidal constant $k_2$ for relativistic stars

We now turn to rotating relativistic stars, with the goal of using their rotational distortions to estimate  $k_2$ . We use the general relativistic, slow-rotation Hartle-Thorne framework [37, 38], as described in [21]. Rotating stars can be characterized by a dimensionless parameter  $\epsilon$ , given by

$$\epsilon = \omega \sqrt{R^3/M}, \quad (\text{A4})$$

which is the ratio between the body's angular velocity and the Keplerian angular velocity at the equator of a non-rotating stellar model (this  $\epsilon$  should not be confused with the post-Newtonian expansion parameter). Even for the fastest-rotating configurations (that is, when we consider corotating binaries at the ISCO)  $\epsilon \lesssim 0.35$  (see the last column of Table V), so a slow-rotation approximation is valid for our purposes. For constant-baryonic mass sequences, the Hartle-Thorne slow-rotation approximation induces an error with respect to the “true” value of the quadrupole moment which depends on the stellar mass and on the EOS. Since the apsidal constant  $k_2$  is proportional to the star's quadrupole moment  $Q$  (see below), our calculation is valid as long as the error in  $Q$  induced by the slow-rotation approximation is small. In Ref. [21] we compared the Hartle-Thorne approximation with rotating neutron star calculations in full general relativity (see eg. Fig. 1 in [21]). From that comparison we conclude that our Hartle-Thorne based values of  $Q$  are good to within a few percent of the “true” values, which is more than acceptable for our estimates.

Following standard conventions (see eg. [34]), we use the relativistic polytropic EOS  $p = \kappa \rho^\Gamma$ , with energy density  $\epsilon = \rho + P/(\Gamma - 1)$ , and work in polytropic units. For  $n \simeq 0.5 - 1$  one obtains models with bulk properties comparable with those of observed neutron stars; polytropic indices  $n < 1$  ( $n > 1$ ) yield stiff (soft) stellar models, respectively. We are interested in fitting numerical sequences of quasidequilibrium binary systems containing neutron stars, which are computed at constant baryonic mass. Correspondingly, we consider rotational corrections along sequences of (isolated) rotating stars with constant baryonic mass.

Given a sequence of rotating models, we can compute the “relativistic” apsidal constant  $k_2$ , defined as

$$k_2 = \frac{3}{2} \frac{Q}{R^5 \omega^2} = \frac{3}{2} \frac{Q}{MR^2}. \quad (\text{A5})$$

for fixed values of  $M/R$ , where  $Q$  is the quadrupole moment of the star as determined from the exterior geometry. The last step makes use of the fact that, in the Hartle-Thorne formalism,  $Q$  and all rotation-dependent quantities (scaling with some power of  $\omega$ ) are computed at the “reference” angular velocity  $\omega = \sqrt{M/R^3}$ . As shown in Appendix B.3 of [6], this is the most natural relativistic generalization of the Newtonian apsidal constant. In fact, we verified that in the Newtonian limit  $M/R \rightarrow 0$  the Hartle-Thorne code reproduces the Newtonian apsidal constants listed in Table III. Notice that since  $Q \propto \epsilon^2$ , and  $k_2 \propto Q/\omega^2$ ,  $k_2$  does not depend on the rotation rate, but only on  $M/R$ . A concise way of presenting the data is by a polynomial least-squares fit (basically a post-Newtonian series) of the form

$$k_2 = \sum_{j=0}^2 k_2^{(j)} (M/R)^j. \quad (\text{A6})$$

The coefficients  $k_2^{(j)}$  are listed in Table IV. We also report the percentage errors of the fits with respect to the numerical calculations,  $\Delta k_2^{\text{max}} = \max[(k_2 - k_2^{\text{num}})/k_2^{\text{num}}]$ : the fit is in excellent agreement with the numerical data for all values of  $n$  and in the whole range of  $M/R$ . For this reason, we used the analytical fits when computing the relativistically corrected apsidal constants to use in the diagnostic equations.

Over the range of compactness factors shown,  $k_2$  decreases by a factor of order two. This gives a small but noticeable shift in the eccentricities inferred from the numerical data, as displayed in Figs. 2 and 3; because the diagnostic baseline shifts toward a point-mass model (smaller  $k_2$ ) the data referred to that baseline (the triangles) shift upward.

TABLE IV: Fitting coefficients for the “relativistic” apsidal constants as defined in Eq. (A6). The fifth column shows the maximum percentage error of the fit with respect to the numerical data, and the last column shows the maximum value of  $M/R$  used in the fit.

$n$	$k_2^{(0)}$	$k_2^{(1)}$	$k_2^{(2)}$	$\Delta k_2^{\text{max}}(\%)$	$(M/R)^{\text{max}}$
1.25	0.194339	-0.773249	0.733840	0.32	0.172
1.00	0.259909	-0.956592	1.052813	0.21	0.214
0.80	0.325098	-1.144687	1.377584	0.23	0.252
2/3	0.375966	-1.296016	1.634947	-0.80	0.278

### 3. Mass and moment of inertia of relativistic stars

For future applications of the PN diagnostic to binaries with rotating neutron stars, it will be useful to have estimates of the variation in the mass and angular momentum of isolated rotating neutron stars, as a function of compactness and angular velocity.

We used the code described in [21] to compute rotational corrections to the gravitational mass of the isolated neutron star as a function of rotation for different values of  $n$ . We assume that the non-rotating model has one of the compactness  $M/R$  values chosen in Table I; this fixes the value of the baryonic mass for our nonrotating model. Then we increase the rotation rate at fixed baryonic mass (along an “evolutionary sequence”) and compute the rotationally corrected gravitational mass

$$M_{\text{rot}} \equiv (1 + \beta) M_{\text{nonrot}}. \quad (\text{A7})$$

More details on our numerical procedure are given in Sec. 3.1 of [21] (the main difference being that there we fix the angular momentum and gravitational mass, here we fix angular velocity and baryonic mass).

For each value of  $n$  and of the nonrotating star’s compactness ( $M/R$ ), we compute 11 models (the nonrotating model and 10 models equispaced in the angular velocity  $\omega$ ). Then we perform a polynomial least-squares fit of  $\beta$  as a function of the star’s angular velocity  $\bar{\omega}$  (expressed in polytropic units):

$$\beta = \sum_{k=1}^3 \beta^{(k)} \bar{\omega}^k. \quad (\text{A8})$$

The fitting coefficients  $\beta^{(k)}$  are listed in Table V.

TABLE V: Fitting coefficients for  $\beta(\omega)$  as defined in Eqs. (A7) and (A8).  $(M/R)_{\epsilon=0}$  is the compactness and  $M$  is the gravitational mass (in polytropic units) of the nonrotating model. The seventh column shows the maximum percentage error of the fit with respect to the numerical data, and the last two columns show the maximum value of  $\bar{\omega}$  or  $\epsilon$  used in the fit.

$n$	$(M/R)_{\epsilon=0}$	$M$	$10^3 \times \beta^{(1)}$	$\beta^{(2)}$	$\beta^{(3)}$	$\Delta\beta^{\max}(\%)$	$\bar{\omega}^{\max}$	$\epsilon^{\max}$
1.25	0.08	0.143165	1.500742	0.321866	1.617628	0.98	0.048	0.316
1.25	0.10	0.164915	0.138509	0.325523	0.740812	0.49	0.058	0.316
1.25	0.12	0.182153	0.277598	0.272061	0.736909	0.46	0.071	0.327
1.25	0.14	0.194658	1.062211	0.207540	0.858382	0.78	0.083	0.329
1.00	0.12	0.122286	-0.072168	0.153656	0.082648	2.61	0.109	0.331
1.00	0.14	0.136233	0.628680	0.126834	0.168151	0.31	0.125	0.339
1.00	0.16	0.147838	0.781091	0.113525	0.172454	1.69	0.143	0.347
1.00	0.18	0.156736	0.518670	0.105391	0.156755	1.32	0.160	0.350
0.80	0.12	0.087240	-0.221682	0.087986	0.013138	0.78	0.152	0.327
0.80	0.14	0.099987	0.534238	0.076339	0.051296	-0.57	0.171	0.335
0.80	0.16	0.111652	0.278734	0.078449	0.034777	-0.53	0.191	0.343
0.80	0.18	0.122021	0.345399	0.075647	0.035287	-0.24	0.208	0.345
2/3	0.14	0.080637	0.794037	0.049246	0.034088	0.59	0.211	0.332
2/3	0.16	0.091591	-0.248756	0.061873	-0.000499	-0.37	0.232	0.340
2/3	0.18	0.101844	0.009904	0.059124	0.008106	-0.43	0.253	0.347
2/3	0.20	0.111209	0.370593	0.055858	0.014234	-0.15	0.274	0.351

Relativistic corrections to the Newtonian moment of inertia, may be useful for the diagnosis of binaries containing rotating bodies, in order to evaluate the total angular momentum (including that of the stars themselves) and such effects as spin-orbit coupling. Following [6] we define a dimensionless factor

$$\alpha \equiv I/(MR^2) = (R_g/R)^2. \quad (\text{A9})$$

The “radius of gyration” is defined as  $R_g = (I/M)^{1/2}$ . In the Hartle-Thorne formalism, to leading order,  $R_g$  does not depend on the rotation rate (see the discussion following Eq. (11) of [21]). In Table VI we provide fitting coefficients for a post-Newtonian inspired power-series expansion for  $\alpha$ , as computed using the Hartle-Thorne formalism:

$$\alpha = \sum_{j=0}^2 \alpha^{(j)} (M/R)^j. \quad (\text{A10})$$

TABLE VI: Fitting coefficients for  $\alpha(M/R)$  as defined in Eqs. (A9) and (A10). The fifth column shows the maximum percentage error of the fit with respect to the numerical data, and the last column shows the maximum value of  $M/R$  used in the fit.

$n$	$\alpha^{(0)}$	$\alpha^{(1)}$	$\alpha^{(2)}$	$\Delta\alpha^{\max}(\%)$	$(M/R)^{\max}$
1.25	0.231893	0.256949	0.065809	0.19	0.172
1.00	0.261297	0.274488	0.349978	0.15	0.214
0.80	0.286378	0.275807	0.569004	-0.07	0.252
2/3	0.303974	0.269094	0.714660	-0.19	0.278



- 
- [1] A. Buonanno, G. B. Cook and F. Pretorius, Phys. Rev. D **75**, 124018 (2007).
  - [2] E. Berti, V. Cardoso, J. A. Gonzalez, U. Sperhake, M. Hannam, S. Husa and B. Brügmann, preprint (arXiv:gr-qc/0703053).
  - [3] J. G. Baker, J. R. van Meter, S. T. McWilliams, J. Centrella and B. J. Kelly, preprint (arXiv:gr-qc/0612024).
  - [4] M. Hannam, S. Husa, U. Sperhake, B. Brügmann and J. A. Gonzalez, preprint (arXiv:0706.1305).
  - [5] T. Mora and C. M. Will, Phys. Rev. D **66**, 101501(R) (2002).
  - [6] T. Mora and C. M. Will, Phys. Rev. D **69**, 104021 (2004).
  - [7] E. Berti, S. Iyer and C. M. Will, Phys. Rev. D **74**, 061503 (2006).
  - [8] L. Blanchet, Phys. Rev. D **65**, 124009 (2002).
  - [9] J. G. Baker, S. T. McWilliams, J. R. van Meter, J. Centrella, D.-I. Choi, B. J. Kelly and M. Koppitz, Phys. Rev. D **75**, 124024 (2007).
  - [10] H. P. Pfeiffer, D. A. Brown, L. E. Kidder, L. Lindblom, G. Lovelace and M. A. Scheel, Class. Quantum Grav. **24**, S59 (2007).
  - [11] S. Husa, M. Hannam, J. A. Gonzalez, U. Sperhake and B. Brügmann, preprint (arXiv:0706.0904).
  - [12] J. D. Grigsby and G. B. Cook, preprint (arXiv:0706.4286).
  - [13] M. Miller, P. Gressman and W.-M. Suen, Phys. Rev. D **69**, 064026 (2004).
  - [14] E. Gourgoulhon, P. Grandclément, K. Taniguchi, J.-A. Marck and S. Bonazzola, Phys. Rev. D **63**, 064029 (2001).
  - [15] K. Taniguchi and E. Gourgoulhon, Phys. Rev. D **66**, 104019 (2002).
  - [16] K. Taniguchi and E. Gourgoulhon, Phys. Rev. D **68**, 124025 (2003).
  - [17] K. Taniguchi, T. W. Baumgarte, J. A. Faber and S. L. Shapiro, Phys. Rev. D **74**, 041502 (2006).
  - [18] K. Taniguchi, T. W. Baumgarte, J. A. Faber and S. L. Shapiro, Phys. Rev. D **75**, 084005 (2007).
  - [19] K. Taniguchi, T. W. Baumgarte, J. A. Faber, and S. L. Shapiro, in preparation.
  - [20] P. Grandclément, Phys. Rev. D **74**, 124002 (2006) [Erratum-ibid. D **75**, 129903 (2007)]
  - [21] E. Berti, F. White, A. Maniopoulou and M. Bruni, MNRAS **358**, 923 (2005).
  - [22] R. A. Brooker and T. W. Olle, MNRAS **115**, 101 (1955).
  - [23] Z. Kopal, *Close Binary Systems* (Chapman and Hall, London, 1959), Chap. 2.
  - [24] Z. Kopal, *Dynamics of Close Binary Systems* (Reidel, Dordrecht, 1978), Chap. 2.
  - [25] T. W. Baumgarte, G. B. Cook, M. A. Scheel, S. L. Shapiro and S. A. Teukolsky, Phys. Rev. Lett. **79**, 1182 (1997).
  - [26] T. W. Baumgarte, G. B. Cook, M. A. Scheel, S. L. Shapiro and S. A. Teukolsky, Phys. Rev. D **57**, 7299 (1998).
  - [27] P. Marronetti, G. J. Mathews and J. R. Wilson, Phys. Rev. D **58**, 107503 (1998).
  - [28] S. Bonazzola, E. Gourgoulhon and J.-A. Marck, Phys. Rev. Lett. **82**, 892 (1999).
  - [29] P. Marronetti, G. J. Mathews and J. R. Wilson, Phys. Rev. D **60**, 087301 (1999).
  - [30] K. Uryu and Y. Eriguchi, Phys. Rev. D **61**, 124023 (2000).
  - [31] K. Uryu, M. Shibata and Y. Eriguchi, Phys. Rev. D **62**, 104015 (2000).
  - [32] M. Shibata and K. Uryu, Phys. Rev. D **64**, 104017 (2001).
  - [33] P. Marronetti and S. L. Shapiro, Phys. Rev. D **68**, 104024 (2003).
  - [34] N. Stergioulas, *Rotating stars in relativity*, Living Reviews in Relativity (2003).
  - [35] T. W. Baumgarte, M. L. Skoge and S. L. Shapiro, Phys. Rev. D **70**, 064040 (2004).
  - [36] M. Caudill, G. B. Cook, J. D. Grigsby and H. P. Pfeiffer, Phys. Rev. D **74**, 064011 (2006).
  - [37] J. B. Hartle, Astrophys. J. **150**, 1005 (1967).
  - [38] J. B. Hartle and K. S. Thorne, Astrophys. J. **153**, 807 (1968).